Pressure broadening and line shifting of atomic strontium $5s^2\ ^1S_0 \rightarrow 5s5p\ ^3P_1$ and $5s5p\ ^3P_{0,1,2} \rightarrow 5s6s\ ^3S_1$ absorption transitions induced by noble-gas collisions

Jeremy C. Holtgrave and Paul J. Wolf
Department of Engineering Physics, Graduate School of Engineering and Management, Air Force Institute of Technology, Wright-Patterson AFB, Ohio 45433-7765, USA
(Received 24 February 2005; published 15 July 2005)

The broadening and shifting of spectral lines induced by collisions with the five noble gases in both the intercombination $5s^2\ ^1S_0 \rightarrow 5s5p\ ^3P_1$ system and the triplet $5s5p\ ^3P_{0,1,2} \rightarrow 5s6s\ ^3S_1$ manifold of Sr are studied using tunable dye laser absorption spectroscopy. Cross sections for impact broadening and line shifting are determined from an examination of the spectral line profiles. These results are utilized in an analysis to compute difference potentials modeled by the Lennard-Jones (6-12) potential and the coefficients C_6 and C_{12} derived from this analysis are reported.

DOI: 10.1103/PhysRevA.72.012711 PACS number(s): 34.20.Gj, 32.70.Jz

INTRODUCTION

The broadening and shifting of atomic spectral lines induced by interactions with a variety of foreign gas perturbers has been extensively studied both experimentally and theoretically for many years and has led to a number of insights in a variety of fields [1]. Studies of line shapes in the presence of foreign gases is of fundamental interest because they contribute to our understanding of long-range interactions between atoms and provide a method to determine local conditions in laboratory plasmas or neutral gas environments. For example, collision-broadened line shapes of metallic lines in solar and stellar atmospheres can provide indications of local conditions (temperature and number density) and have even been used to determine the surface gravity of stars by examining calcium atomic lines perturbed by hydrogen atoms [2]. The collision-broadening cross section is essential for describing radiation transport in gaseous electronics and, along with the line-shifting cross section, has application to narrowband blocking filters used in remote sensing [3,4]. More recently, a number of spectral lines in the alkali-metal and alkaline-earth-metal atoms are in use or being considered for high-precision frequency standards [5], and understanding line perturbations is important for determining the operating characteristics of devices using these transitions [6]. Singly ionized species have been extensively explored for this application, but there is new interest in utilizing neutral atoms. Strontium, in particular, has attracted interest as a candidate for atomic clocks based on optical frequency transitions [7–10].

The study of line shapes from transitions in strontium has been rather sparse. Much of the earlier work focused on the $5s^2\ ^1S_0 \rightarrow 5s5p\ ^1P_1$ resonance transition at 460.7 nm as shown in Fig. 1. Farr and Hindmarsh [11] studied the absorption line shapes for this resonance transition perturbed by He and Ar. They extracted line-broadening and line-shifting rate coefficients and used them to compute difference potentials between the two states of interest. They utilized the Lennard-Jones (6-12) description to model the difference potential and, subsequently, determined values for the attractive and repulsive terms C_6 and C_{12} from their analysis. Other experimental and theoretical studies followed this initial work in attempts to corroborate Farr and Hindmarsh's results and provide a consistent and complete understanding of the broadening and shifting process of the strontium resonance line in the presence of noble gases [12–16]. More recently, Kerkeni *et al.* [17] have computed broadening cross sections for the alkaline-earth-metal atoms in collisions with H atoms. Crane *et al.* reported the only study of collision broadening of a Sr intercombination band that we are aware of to date [3]. In their work, they determined broadening cross sections for the $5s^2\ ^1S_0 \rightarrow 5s5p\ ^3P_1$ in collisions with Ar, Ne, and the ground-state neutral Sr vapor and subsequently computed the Lennard-Jones interaction C_6 and C_{12} coefficients.

In this work, we report the results of a systematic study of collision broadening and line shifting of spectral features for the $5s^2\ ^1S_0 \rightarrow 5s5p\ ^3P_1$ transition at 689.5 nm and the $5s5p\ ^3P_{0,1,2} \rightarrow 5s6s\ ^3S_1$ transitions at 679.3, 688.0, and 707.2 nm, respectively in ^{88}Sr using the five noble gases as collision partners, thereby extensively extending the work reported by Crane *et al.* [3]. Figure 1 shows the relevant energy levels and transitions for strontium. We experimen-

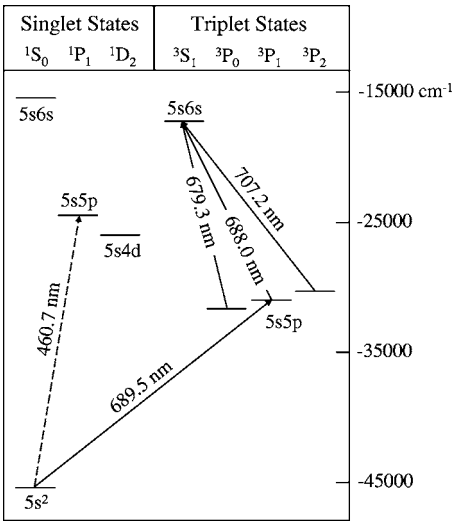

FIG. 1. Lower-energy electronic manifold of atomic strontium. The transitions of interest to this study are identified by the solid arrowed lines.

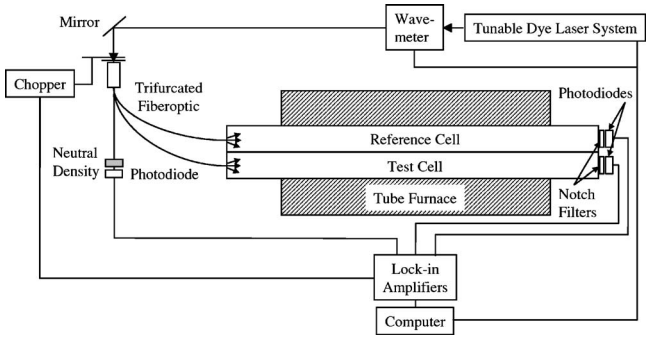

FIG. 2. Schematic diagram of experimental apparatus.

tally map the line shapes using absorption spectroscopy with a narrowband tunable dye laser. We confine our investigation to the core region of the spectral lines where the impact approximation remains valid, yielding a Lorentzian profile for the line shape, and subsequently determine collision-broadening rate coefficients. We were able to extract both line-broadening and line-shifting cross sections from the absorption line shapes and we use this information to create difference potentials modeled by the Lennard-Jones (6-12) potential and, thereby, determine the C_6 and C_{12} coefficients.

EXPERIMENTAL METHOD

Our experimental arrangement is shown in Fig. 2. Strontium vapor cells were constructed with tantalum-foil-lined quartz cylinders, each 1.83 m long and 3.8 cm in diameter. A strontium vapor was created inside both cells by placing strontium granules (Aldrich, 99% pure) in the center of each cylinder and heating the central region of the cylinders in a tube furnace. The central section of each tube, 76 cm in length, was embedded in the furnace while the remaining length protruded equally from both ends of the furnace. This arrangement was required to prevent a Sr film from being deposited on the cell windows and interfering with the optical absorption measurements. Each cell was connected to a vacuum pump, a gas handling system, and MKS Baratron capacitance manometers which monitored the pressures. The base pressure in each cell was 10^{-3} Torr. One of the two cells was used as a reference cell which contained Sr vapor whose absorption line shape was utilized as a reference for the center-line frequency for the transition under study. The pressure in this cell remained constant during a given set of trials. The second cell (test cell) contained Sr vapor which was exposed to various noble gases at pressures ranging from 20 to 1000 Torr, and Sr signals from the test cell were used to observe the broadening and shifting of the absorption line profiles. Research-grade rare gases with a minimum purity of 99.995% were used without additional purification.

Spectral line shapes were recorded by scanning the output of a Coherent 899-21 ring dye laser over the Sr absorption transitions of interest. The effective bandwidth of the laser was nominally 1 MHz. When pumped simultaneously by the 488 and 514.5 nm lines from an Ar ion laser, the Pyradine-1 laser dye produced radiation in the wavelength range between 780 and 680 nm with a corresponding output power of

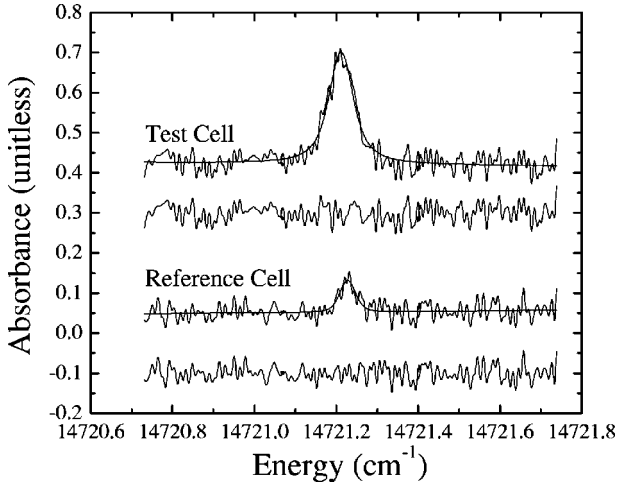

FIG. 3. Spectral absorption profiles of the strontium $5s5p\ ^3P_0 \rightarrow 5s6s\ ^3S_1$ transition perturbed by argon along with a Voigt fit to the line shapes. The upper trace is obtained from the test cell with 140.0 Torr of Ar and the lower figure is an absorption profile from the reference cell. Residuals of the fit are displayed beneath each profile. The test-cell line profile and residuals are displaced upward and the reference-cell residuals downward for clarity.

$\sim$100–200 mW, respectively. In practice, we used neutral-density filters to reduce the laser power to prevent detector saturation. The ring laser was programmed to continuously scan over a 30 GHz frequency range with the peak of the absorption profile centered in each scan. The laser beam was chopped at a frequency of 330 Hz and then split into three parts by a trifurcated fiber-optic cable. One laser beam was directed into the reference cell, the second into the test cell, and the third beam was incident on a bare detector to monitor the laser intensity. Laser intensities were detected with Hamamatsu-type S2281 silicon photodiodes that were covered with Corion P70-700-F notch filters and placed at the exit of the reference and test cells. These filters allowed optical signals between 647.3 nm and 735.5 nm to pass to the detector, significantly reducing the background created by the heating elements in the tube furnace. The signals from the three photodiodes were individually registered on separate Stanford Research Systems model SR850 lock-in amplifiers tuned to the chopping frequency. Data from the lock-in amplifiers were then sent to the computer controlling the dye laser so that intensity as a function of laser frequency could be recorded.

Each run of the experiment provided two absorption profiles: one from the reference cell and the other from the test cell. For the line-broadening and -shifting studies on the $5s^2\ ^1S_0 \rightarrow 5s5p\ ^3P_1$ transition, a tube furnace with dial setting of 728 K provided sufficient Sr density to produce a signal that was approximately 75%–95% of total absorption. For a system in equilibrium, the vapor pressure of atomic strontium at this temperature was approximately 10^{-4} Torr and the signal-to-noise ratio ranged from about 20:1 at the lowest perturbing gas pressure to 3:1 at the highest pressures. In contrast, we required a furnace temperature setting of 1473 K to study the line shapes of the $5s5p\ ^3P_{0,1,2} \rightarrow 5s6s\ ^3S_1$ transitions and obtain comparable absorption sig-

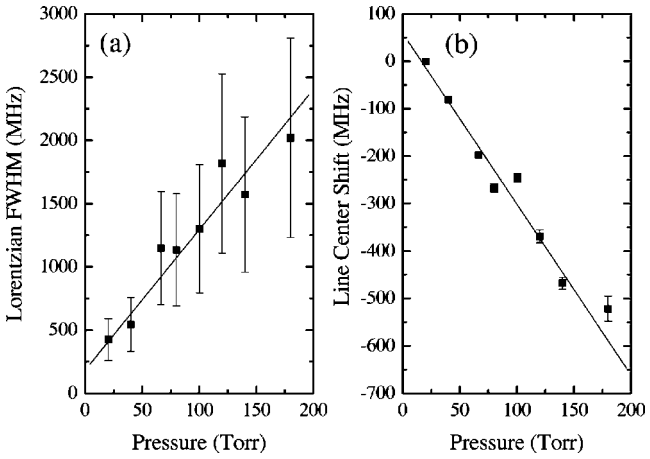

FIG. 4. A plot of (a) the Lorentzian linewidths (FWHM) and (b) the line-center shifts for the $5s5p\ ^3P_0 \rightarrow 5s6s\ ^3S_1$ transition of Sr as a function of Ar pressure. Linear fits are superimposed upon the data.

nals. In this case, the Sr vapor pressure is reported to be about 100 Torr [18]. Since we relied on thermally populating the $5s5p\ ^3P_{0,1,2}$ states, this drastic increase in operating temperature was necessary to sufficiently raise the strontium vapor pressure and, therefore, the number density, to compensate for the low population of atoms in the initial state of the transition. (The population in the ^3P states was about 10^{-6} of the $5s^2\ ^1S_0$ ground state.) Here, the signal-to-noise ratios varied from 70:1 (low noble-gas pressures) to 5:1 (high noble-gas pressures) during the course of the experiment. In addition, the reference cell at the 1473 K dial setting was backfilled to 30 Torr of the noble gas, being used in the broadening and shifting study to reduce diffusion of the Sr vapor to cooler regions of the cell. In contrast, the reference cell contained no backing gas for the lower-temperature study. The time frame over which data were collected under these experimental conditions was limited by the diffusion of Sr from the heated region of the cell and lasted approximately 45 min. The 30 GHz scans were completed in 1 min and data points were separated by 25 MHz, thereby producing 1200 data points per transition profile. The transition profiles in the test cell were recorded using four to eight different noble-gas pressures ranging from a few mTorr to approximately one atmosphere, while pressure in the reference cell was held constant.

RESULTS

Figure 3 displays a sample spectral line profile for the $5s5p\ ^3P_0 \rightarrow 5s6s\ ^3S_1$ transition with 140.0 Torr of argon. The upper trace illustrates data obtained from the test cell and the lower trace is from the reference cell. A Voigt profile has been used to fit each line shape using a multivariable nonlinear least squares fitting procedure. The Voigt profile is defined in Eq. (1):

$$I_V(x) = a_0 \frac{\ln(2)}{\sqrt{\pi^5}} \frac{1}{c} \frac{\delta x_L}{\delta x_G^2} \int_{-\infty}^{\infty} \frac{e^{-y^2}}{\{[2\sqrt{\ln(2)}(x - x_0)/\delta x_G] - y^2\}^2 + \ln(2)(\delta x_L/\delta x_G)^2} dy. \quad (1)$$

This line-shape function has four parameters that can float independently during a fit. Specifically, the parameters of the fit are the Doppler (Gaussian) and Lorentzian full width at half maximum (FWHM) linewidths δx_G and δx_L, respectively; the pressure-dependent line-center frequency x_0; and an amplitude scaling factor a_0, which is proportional to the product of the column density and the transition oscillator strength. The Lorentzian linewidths produce the collision-induced line-broadening rates.

The Gaussian component of the Voigt profile provided us with the means to determine the gas temperatures in both the reference and test cells. First, we acquired line profiles from each cell under identical initial conditions (i.e., no broadening gas in the test cell), fitted these profiles with the Voigt line shape of Eq. (1), and extracted the temperatures from the Doppler widths. On average, the gas temperature was 660 ± 47 K in the low-temperature study and 1390 ± 243 K in the high-temperature study, and the temperatures in the two cells differed by no more than 5% from each other.

Since the temperatures in both cells were statistically equal to within experimental error, the reference-cell line profiles were used to establish and fix a Gaussian linewidth to be used in the Voigt fits to the test-cell line profiles, thereby reducing the number of free fitting parameters. We allowed all four parameters to float during the fits to the reference-cell line profiles and then averaged the Gaussian linewidths for each set of trials. This average Gaussian linewidth was then used as a fixed parameter in the test-cell line profile fits. Figure 3 shows the reference- and test-cell line profiles fitted to the Voigt line-shape function of Eq. (1). Also, the residuals are given below each profile and fit. They appear random, which indicates that the Voigt profile adequately models the line-shape function.

Atomic strontium has four isotopes with atomic numbers 88, 87, 86, and 84. ^{88}Sr is the most abundant (82.58%) naturally occurring isotope while the remaining isotope abundances are, respectively, 7%, 9.86%, and 0.56%. In addition, ^{87}Sr has hyperfine structure due to the 9/2 spin of the nucleus. Although isotopes other than ^{88}Sr are much less abundant, their presence could influence the spectral line shapes observed here. Ignoring the least abundant isotope, we fitted the experimental line shapes using three Voigt profiles to account for the hyperfine structure in ^{87}Sr ($F = 11/2$, 9/2, and 7/2) while keeping the Gaussian widths constant. We find a less than 3% difference in the value of the Lorentzian widths produced in this fit as compared to a single Voigt

TABLE I. Pressure-broadening and line-shifting rate coefficients and cross sections for the $5s^2\ ^1S_0 \rightarrow 5s5p\ ^3P_1$ transition at 689.5 nm in ^{88}Sr. The average Sr temperature extracted from the Doppler-broadened linewidths was 660±47 K. The errors quoted for the rate coefficients and cross sections are 1σ from the mean.

Broadening gas	k_p (MHz/Torr)	σ_p (10^{-14} cm^2)	k_s (MHz/Torr)	σ_s (10^{-14} cm^2)
He	7.58 (0.34)	0.89 (0.04)	+1.23 (0.06)	+0.290 (0.015)
Ne	5.20 (0.26)	1.27 (0.06)	−0.64 (0.04)	−0.31(0.02)
Ar	4.90 (0.07)	1.57 (0.02)	−1.45 (0.04)	−0.929 (0.026)
Kr	6.17 (0.31)	2.44 (0.12)	−1.53 (0.05)	−1.21 (0.04)
Xe	6.88 (0.45)	3.01 (0.20)	−1.51 (0.03)	−1.32 (0.03)

fit and the values are within the statistical uncertainties of the fit. We have also fitted the line shapes to a double Voigt function, one to account for the ^{86}Sr isotope, and we find no statistical difference in the results. Therefore, a single Voigt function provides an accurate description of the line profiles in this study since we observe no contribution to the line profiles from the other Sr isotopes.

The pressure-broadening and line-shifting rates have been determined by applying the fitting process described above to the line profiles. Since both δx_L and the line-center difference between the reference and test cells (line-center shift) are linearly dependent on the number density, we plot the line-broadening and line-shifting rates against the pressure of the foreign gas. The slopes of a linear fit to these data, weighted by the experimental uncertainties, produce the pressure-broadening (k_p) and line-shifting (k_s) rate coefficients. Figure 4 shows a plot of the data for the $5s5p\ ^3P_0 \rightarrow 5s6s\ ^3S_1$ transition perturbed by argon. The error bars shown in the figure are statistical uncertainties from the fits to the line shapes. For the data in Fig. 4, the broadening rate coefficient k_p is 11.1±1.1 MHz/Torr and the line-shifting rate coefficient k_s is −(3.60±0.30) MHz/Torr. A positive line-center shift indicates a transition frequency shift to higher energies with increasing pressure while a negative line-center shift indicates a peak shift toward the red end of the spectrum. That is, the collision between the noble-gas atom and the Sr atom during its transition shifts the energy levels to either increase the separation between the states (positive shift) or decrease the separation (negative shift). Tables I–IV summarize the pressure-broadening and line-shifting rate coefficients measured here.

The temperature dependences inherent in the rate coefficients were removed by converting the pressure-broadening and line-shifting rate coefficients to cross sections using Eqs. (2) and (3), respectively [19],

$$\sigma_p = \sqrt{\frac{\pi^3 \mu k_B T c^2}{8}} k_p, \tag{2}$$

$$\sigma_s = 2\sqrt{\frac{\pi^3 \mu k_B T c^2}{8}} k_s. \tag{3}$$

In these expressions, σ_p is the pressure or impact broadening cross section, σ_s is the line-shifting cross section, μ is the reduced mass of the strontium–noble-gas pair, k_B is Boltzmann's constant, T is the temperature, and c is the speed of light. The converted rate coefficients are also presented in Tables I–IV.

DISCUSSION

It is difficult to compare our results of foreign-gas broadening and line shifting in ^{88}Sr to others because of the scantiness of pressure-broadening data in Sr, other than its resonance transition. To the best of our knowledge, the only other study reporting pressure broadening in Sr other than in the resonance transition is that of Crane *et al.* [3]. In their investigations, Crane *et al.* determined pressure-broadening cross sections for the $5s^2\ ^1S_0 \rightarrow 5s5p\ ^3P_1$ transition in Sr with Ar and Ne. Their value for Ar, $\sigma_p = (1.52 \pm 0.18) \times 10^{-14}$ cm^2, is

TABLE II. Pressure-broadening and line-shifting rate coefficients and cross sections for the $5s5p\ ^3P_0 \rightarrow 5s6s\ ^3S_1$ transition at 679.3 nm in ^{88}Sr. The average Sr temperature extracted from the Doppler-broadened linewidths was 1390±243 K. The errors quoted for the rate coefficients and cross sections are 1σ from the mean.

Broadening gas	k_p (MHz/Torr)	σ_p (10^{-14} cm^2)	k_s (MHz/Torr)	σ_s (10^{-14} cm^2)
He	11.8 (1.5)	1.98 (0.25)	+1.92 (0.20)	+0.65 (0.07)
Ne	4.68 (0.91)	1.63 (0.32)	−0.75 (0.07)	−0.52 (0.05)
Ar	11.1 (1.1)	4.99 (0.48)	−3.60 (0.30)	−3.24 (0.27)
Kr	10.4 (1.4)	5.86 (0.78)	−3.11 (0.12)	−3.50 (0.13)
Xe	10.9 (0.3)	6.80 (0.20)	−3.70 (0.03)	−4.60 (0.03)

TABLE III. Pressure-broadening and line-shifting rate coefficients and cross sections for the $5s5p\ ^3P_1 \rightarrow 5s6s\ ^3S_1$ transition at 688.0 nm in ^{88}S. The average Sr temperature extracted from the Doppler-broadened linewidths was 1390±243 K. The errors quoted for the rate coefficients and cross sections are 1σ from the mean.

Broadening gas	k_p (MHz/Torr)	σ_p (10^{-14} cm^2)	k_s (MHz/Torr)	σ_s (10^{-14} cm^2)
He	14.6 (0.8)	2.45 (0.14)	+1.69 (0.16)	+0.57 (0.05)
Ne	4.88 (0.68)	1.69 (0.24)	−0.43 (0.09)	−0.30 (0.06)
Ar	10.3 (1.5)	4.64 (0.67)	−3.34 (0.02)	−3.00 (0.02)
Kr	9.51 (0.96)	5.34 (0.54)	−2.91 (0.19)	−3.26 (0.22)
Xe	11.7 (2.6)	7.30 (1.6)	−2.90 (0.42)	−3.61 (0.52)

equal to the value reported here to within experimental error with a less than 3% difference in the average value for the cross section. In contrast, their value for Ne was $(0.98\pm0.12)\times10^{-14}$ cm^2 which translates to a 23% difference and does not agree well with our results to within experimental error. Crane *et al.* did not measure line shifting.

The collision-broadening cross sections shown in Tables I–IV show a systematic increase in their values with increased collision reduced mass. The heavier noble gases tend to be more efficient in broadening the Sr absorption lines studied here. Efficiency, as defined here, is the ratio of the broadening cross section to a calculated gas kinetic value for the Sr–noble-gas pair. (The gas kinetic cross sections for He—Sr to Xe—Sr are, respectively, 3.1×10^{-15}, 3.99×10^{-15}, 4.71×10^{-15}, 4.91×10^{-15}, and 3.1×10^{-15} cm^2.) This trend could be attributed to the polarizability of the noble-gas atom. That is, the polarizability of the noble gases increases from He to Xe and the larger polarizabilty of the collision partner could induce stronger interactions via dispersion forces and, therefore, produce stronger perturbations during the absorption process with the Sr atom. The broadening cross sections for the $5s5p\ ^3P_{0,1,2} \rightarrow 5s6s\ ^3S_1$ transitions perturbed by the noble gases are plotted in Fig. 5 as a function of the angular momentum quantum number J of the initial state. The data indicate that the broadening cross sections show no dependence on angular momentum of the atom to within experimental error, a trend seen repeatedly in the collision broadening of molecular absorption lines [20].

These pressure-broadening and line-shifting results provide the means to extract a set of fundamental information about the interactions between Sr and the various noble gases. In particular, the prescription of Hindmarsh and Farr [19] provides a method to compute difference potentials, which are defined as the energy difference between two atomic states, using the pressure-broadening and line-shifting cross sections. If the Lennard-Jones potential is used to represent the difference potential, then the van der Waals constants C_6 and C_{12} can be extracted from the analysis.

The difference potentials between atomic strontium energy states as they are perturbed by interacting species are related to the line-broadening and -shifting cross sections by the following expressions:

$$\sigma_p = 2\pi \int_0^\infty [1 - \cos\ \eta(\rho)]\rho\, d\rho, \tag{4}$$

$$\sigma_s = 2\pi \int_0^\infty \sin\ \eta(\rho)\rho\, d\rho. \tag{5}$$

The species absorbing radiation is modeled as an oscillating electric charge and, during a collision, the term $\eta(\rho)$ represents the phase perturbation of the electric field as a function of impact parameter ρ, and can be expressed as

$$\eta(\rho) = \frac{2}{\hbar\langle v\rangle} \int_\rho^\infty \frac{V(r) r\, dr}{\sqrt{r^2 - \rho^2}} \tag{6}$$

where $V(r)$ is the difference potential, $\langle v\rangle$ is the average relative velocity between absorbing and perturbing species, and r is the separation between the Sr and noble-gas atoms.

TABLE IV. Pressure-broadening and line-shifting rate coefficients and cross sections for the $5s5p\ ^3P_2 \rightarrow 5s6s\ ^3S_1$ transition at 707.2 nm in ^{88}Sr. The average Sr temperature extracted from the Doppler-broadened linewidths was 1390±243 K. The errors quoted for the rate coefficients and cross sections are 1σ from the mean.

Broadening gas	k_p (MHz/Torr)	σ_p (10^{-14} cm^2)	k_s (MHz/Torr)	σ_s (10^{-14} cm^2)
He	10.9 (1.4)	1.83 (0.24)	+2.06 (0.12)	+0.69 (0.04)
Ne	4.72 (0.35)	1.64 (0.12)	−0.45 (0.03)	−0.32 (0.02)
Ar	9.39 (0.70)	4.22 (0.31)	−3.95 (0.13)	−3.55 (0.12)
Kr	10.37 (0.68)	5.83 (0.38)	−2.80 (0.10)	−3.14 (0.11)
Xe	11.09 (0.46)	6.90 (0.29)	−3.63 (0.11)	−4.52 (0.14)

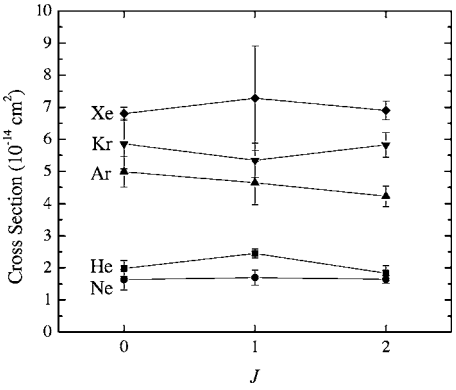

FIG. 5. A plot of the pressure-broadening cross sections for the $5s5p\ ^3P_{0,1,2} \rightarrow 5s6s\ ^3S_1$ transitions of Sr perturbed by the noble gases as a function of the initial-state total angular momentum quantum number J.

The Lennard-Jones (6–12) potential is often a useful way of expressing the difference potential because it involves two relatively intuitive terms: the attractive or van der Waals constant C_6 and the repulsive nuclear term C_{12}, where

$$V(r) = \frac{C_{12}}{r^{12}} - \frac{C_6}{r^6}. \tag{7}$$

If this expression is used in Eq. (6), then the line-broadening and -shifting cross sections are related directly to the difference potential constants by the following equations:

$$\sigma_p = 8\pi \left(\frac{3\pi}{8} \frac{C_6}{\hbar \langle v \rangle} \right)^{2/5} B(\alpha), \tag{8}$$

$$\sigma_s = 2\pi \left(\frac{3\pi}{8} \frac{C_6}{\hbar \langle v \rangle} \right)^{2/5} S(\alpha), \tag{9}$$

where

$$B(\alpha) = \int_0^\infty \sin^2 \left\{ \frac{1}{2} \left(\frac{\alpha}{r^{11}} - \frac{1}{r^5} \right) \right\} r\, dr, \tag{10}$$

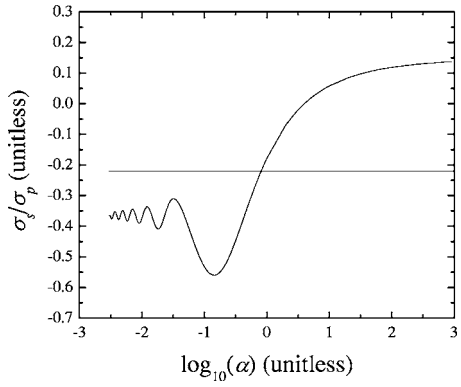

FIG. 6. The ratio of the line-shifting cross section to the pressure-broadening cross section is plotted vs $\log_{10}(\alpha)$. The experimentally derived ratio for the $5s^2\ ^1S_0 \rightarrow 5s5p\ ^3P_1$ transition perturbed by Xe is indicated by the horizontal line showing the intersection with the computed curve.

TABLE V. A summary of the Sr–noble-gas Lennard-Jones constants C_6 and C_{12} used to construct the difference potentials.

Noble gas	Transition	C_6 (10^{-58} erg cm^6)	C_{12} (10^{-101} erg cm^{12})
He	$^1S_0 \rightarrow {}^3P_1$	0	0.186
Ne		0.912	1.285
Ar		1.860	3.473
Kr		4.04	31.276
Xe		5.80	89.26
He	$^3P_0 \rightarrow {}^3S_1$	0	23
Ne		2.73	7.50
Ar		48.9	2730
Kr		56.3	5410
Xe		77.99	10670
He	$^3P_1 \rightarrow {}^3S_1$	1.58	69.8
Ne		2.36	8.52
Ar		40.8	1840
Kr		45.2	3250
Xe		80	16480
He	$^3P_2 \rightarrow {}^3S_1$	0	20.1
Ne		2.231	7.19
Ar		32.11	900
Kr		52.9	5341
Xe		79.8	11700

$$S(\alpha) = \int_0^\infty \sin \left(\frac{\alpha}{r^{11}} - \frac{1}{r^5} \right) r\, dr, \tag{11}$$

and

$$\alpha = \frac{63\pi}{256} \left(\frac{8}{3\pi} \right)^{11/5} \langle v \rangle^{6/5} \frac{C_{12} \hbar^{6/5}}{C_6^{11/5}}. \tag{12}$$

A solution can be obtained by first computing both $S(\alpha)$ and $B(\alpha)$ and plotting the ratio of the line-shifting cross section to the pressure-broadening cross section vs $\log_{10}(\alpha)$ where $\sigma_s/\sigma_p = S(\alpha)/4B(\alpha)$. A sample plot is shown in Fig. 6. Next, we take the experimentally derived ratio of the two cross sections and find the intersection with the computed curve, also shown in Fig. 6. The value at the intersection of the experimental ratio and the computed curve allows us to extract the parameter α and provides the relationship between $S(\alpha)$ and $B(\alpha)$. The van der Waals constant C_6 can then be determined using Eqs. (8) and (9) and the value for C_{12} can be derived from Eq. (12). For collisions between He and Sr, the ratio of the broadening to line-shifting cross sections approaches the asymptotic limit and, therefore, the potential is treated as purely repulsive. Table V summarizes the Lennard-Jones coefficients for each noble-gas–Sr system derived from these analyses and the difference potentials are plotted in Fig. 7. The difference potentials of Fig. 7 show shallow bound states for all the Sr–noble-gas pairs except for He. The He—Sr difference potential is repulsive in all cases and the bound systems are all very weak with well depths below

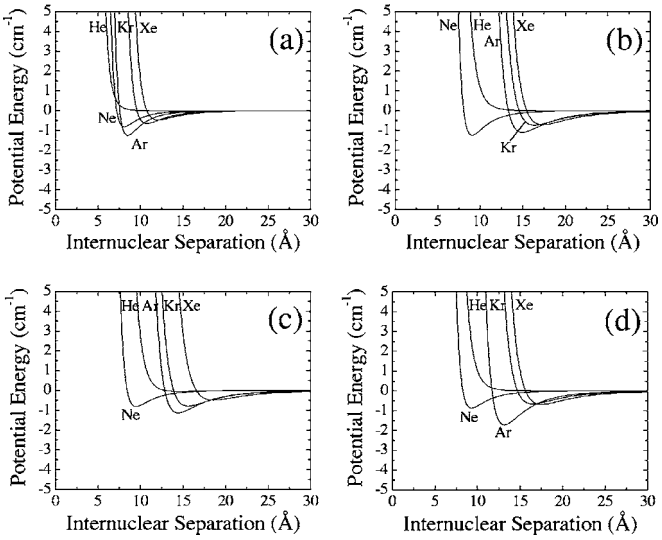

FIG. 7. Difference potential energy curves for Sr–noble-gas collision systems plotted against internuclear separation: (a) $5s^2\ ^1S_0 \leftrightarrow 5s5p\ ^3P_1$; (b) $5s5p\ ^3P_0 \leftrightarrow 5s6s\ ^3S_1$; (c) $5s5p\ ^3P_1 \leftrightarrow 5s6s\ ^3S_1$; and (d) $5s5p\ ^3P_2 \leftrightarrow 5s6s\ ^3S_1$. The Lennard-Jones (6-12) potential was used to model the difference potentials.

2 cm^{-1}. These qualitative results are not entirely unreasonable in light of computations performed by Lovallo and Klobukowski [21]. In their theoretical study, Lovallo and Klobukowski computed Sr—He pair potentials using the ground states of both atoms. They predict a potential with only three rovibrational states and one that is very shallow with an approximate well depth of only 2 cm^{-1} which is indicative of a weakly bound system. In addition, difference potentials calculated for the Sr resonance transition ($^1S_0 \rightarrow {}^1P_1$ with He also produce a very weakly bound system [11–13]. The well depths in the resonance transition studies, however, show depths increasing with the mass (and polarizability) of the noble-gas collision partner. We observe the opposite effect here, which remains unexplained until further studies are performed.

SUMMARY

We have utilized tunable dye laser absorption spectroscopy for measuring Lorentzian linewidths and line-center frequencies of collisionally broadened, radiative transitions in ^{88}Sr. In particular, we acquired spectral line shapes in the intercombination band $5s^2\ ^1S_0 \rightarrow 5s5p\ ^3P_1$, and in the triplet manifold $5s5p\ ^3P_{0,1,2} \rightarrow 5s6s\ ^3S_1$, of strontium. The line profiles were fitted to a Voigt function to extract the Lorentzian linewidths and the line-center frequencies and these values were subsequently used to determine collision-broadening and line-shifting cross sections induced by collisions with the five noble gases. Generally, the collision-broadening cross sections increased with increasing mass of the collision partner. The line-shifting cross sections were positive for helium (greater separation between the states) and negative for the other noble gases possibly due to a small or nonexistent attractive difference potential terms for the Sr—He system. We used these results to compute difference potentials using a classical impact model and the Lennard-Jones potential to model for the difference potential for the various Sr–noble-gas pairs. We also reported the Lennard-Jones parameters C_6 and C_{12} for each collision pair and transition.

ACKNOWLEDGMENTS

We would like to thank Professor Glen P. Perram for stimulating discussions during the course of this work. We would also like to gratefully acknowledge the financial support from the Air Force Office of Scientific Research.

[1] J. Szudy and W. E. Baylis, Phys. Rep. **266**, 127 (1996).
[2] A. N. Spielfiedel, N. Feautrier, G. Chambaud, and B. Levy, J. Phys. B **24**, 4711 (1991).
[3] J. K. Crane, M. J. Shaw, and R. W. Presta, Phys. Rev. A **49**, 1666 (1994).
[4] E. Kuchta, R. J. Alvarez II, Y. H. Li, D. A. Krueger, and C. Y. She, Appl. Phys. B: Photophys. Laser Chem. **50**, 129 (1990).
[5] A. Bauch and H. R. Telle, Rep. Prog. Phys. **65**, 789 (2002).
[6] P. J. Oreto, Y.-Y. Jau, A. B. Post, N. N. Kuzma, and W. Happer, Phys. Rev. A **69**, 042716 (2004).
[7] G. Ferrari, P. Cancio, R. Drullinger, G. Giusfredi, N. Poli, M. Prevedelli, C. Toninelli, and G. M. Tino, Phys. Rev. Lett. **91**, 243002 (2003).
[8] I. Courtillot, A. Quessada, R. P. Kovacich, J.-J. Zondy, A. Landragin, G. Santarelli, A. Clairon, and P. Lemonde, IEEE Trans. Instrum. Meas. **52**, 255 (2003).
[9] I. Courtillot, A. Quessada, R. P. Kovacich, A. Brusch, D. Kolker, J.-J. Zondy, G. D. Rovera, and P. Lemonde, Phys. Rev. A **68**, 030501(R) (2003).
[10] J. L. Hall, M. Zhu, and P. Buch, J. Opt. Soc. Am. B **6**, 2194 (1989).
[11] J. M. Farr and W. R. Hindmarsh, J. Phys. B **4**, 568 (1971).
[12] L. N. Shabanova, Opt. Spektrosk. **36**, 13 (1974).
[13] S. Y. Wang and S. Y. Ch'en, J. Quant. Spectrosc. Radiat. Transf. **22**, 87 (1979).
[14] H. Harima, Y. Fukuzo, K. Tachibana, and Y. Urano, J. Phys. B **14**, 3069 (1981).
[15] A. Z. Devdariani, Y. I. Ponomarev, and Y. N. Sebyakin, Opt. Spektrosk. **59**, 26 (1985).
[16] Y. C. Chan and J. A. Gelbwachs, J. Phys. B **25**, 3601 (1992).
[17] B. Kerkeni, P. S. Barklem, A. Spielfiedel, and N. Feautrier, J. Phys. B **37**, 677 (2004).
[18] *CRC Handbook of Chemistry and Physics*, 76th ed., edited by D. R. Linde, (CRC Press, Boca Raton, FL, 1996).
[19] W. R. Hindmarsh and J. M. Farr, *Progress in Quantum Electronics* (Pergamon Press, Oxford, 1972), Vol. 2, p. 141.
[20] See, for example, R. S. Pope, P. J. Wolf, and G. P. Perram, J. Mol. Spectrosc. **223**, 439 (2003).
[21] C. C. Lovallo and M. Klobukowski, Chem. Phys. Lett. **373**, 439 (2003).